

Electron capture decay of ^{116}In and nuclear structure of double β decays

M. Bhattacharya,¹ A. García,¹ M. M. Hindi,² E. B. Norman,³ C. E. Ortiz,¹ N. I. Kaloskamis,^{1,*} C. N. Davids,⁴
O. Civitarese,⁵ and J. Suhonen⁶

¹University of Notre Dame, Notre Dame, Indiana 46556

²Physics Department, Tennessee Technological University, Cookeville, Tennessee 38505

³Nuclear Science Division, Lawrence Berkeley National Laboratory, Berkeley, California 94720

⁴Physics Division, Argonne National Laboratory, Argonne, Illinois 60439

⁵Department of Physics, University of La Plata, C. C. 67, 1900-La Plata, Argentina

⁶Department of Physics, University of Jyväskylä, P.O. Box 35, SF-40351, Jyväskylä, Finland

(Received 27 March 1998)

Quasiparticle-random-phase-approximation (QRPA) calculations of double β decays have not been able to reproduce data in the $A = 100$ system. We propose the $A = 116$ system—because of its smaller deformation—as a simpler system to test QRPA calculations. We present results of two experiments we performed, which determine the electron-capture-decay branch of ^{116}In to be $(2.27 \pm 0.63) \times 10^{-2}\%$, from which we deduce $\log ft = 4.39_{-0.15}^{+0.10}$. We present QRPA calculations and compare their predictions to experimental data. Finally we use these calculations to predict the 2ν double- β -decay rate of ^{116}Cd to the ground and excited states of ^{116}Sn . [S0556-2813(98)04608-1]

PACS number(s): 27.60.+j, 21.10.Re, 25.40.Lw, 23.40.-s

I. MOTIVATION

In order to translate results of neutrinoless (0ν) double β decays into coupling constants representing physics beyond the standard model, one needs knowledge of the associated nuclear wave functions. The wave functions have been calculated for the different candidates using two approaches: weak-coupling shell-model calculations based on G -matrix nucleon-nucleon interactions [1,2] and quasiparticle-random-phase-approximation (QRPA) calculations [3–9]. One can test the accuracy of these calculations by comparing calculations to measured two-neutrino (2ν) decay rates. The operator involved in the 2ν decay mode is the Gamow-Teller operator which, for $0^+ \rightarrow 0^+$ double β decays, connects the initial and final states via virtual transitions to $J^\pi = 1^+$ states in the intermediate nucleus, only. The 0ν -mode operators, on the other hand, connect to all states in the intermediate nucleus. For this reason this comparison is not a direct test of the accuracy of the 0ν -rate calculations, but can be taken as a necessary condition for the reliability of the calculations.

Weak-coupling shell-model calculations reproduce 2ν experimental decay rates with varying degrees of success [1,2] but are not available for all double- β -decay candidates. On the other hand, QRPA calculations are available for all double- β -decay candidates but they can reproduce experimental decay rates only by fitting a parameter which controls the particle-particle proton-neutron interaction strength [6,7].

One way to test these models is to find a nucleus in which one can measure not only the double- β -decay rates, but also some of the single- β -decay matrix elements. One such can-

didate is the $A = 100$ [$^{100}\text{Mo}(0^+) - ^{100}\text{Tc}(1^+) - ^{100}\text{Ru}(0^+)$] system. A very stringent test of QRPA calculations has been recently performed by Griffiths and Vogel [10] using this system. The authors there tried to reproduce five observables in the above system: the 2ν double- β -decay rates to the ground and excited 0^+ states in ^{100}Ru and the three single- β -decay matrix elements connecting the initial and final states to the 1^+ ground state of ^{100}Tc . The calculations failed to reproduce all the observables simultaneously. Another theoretical study of the same system using realistic interactions was reported in Ref. [11] with similar results. A possible reason for QRPA calculations not being able to reproduce the data for the $A = 100$ system could be the fact that, for the $A = 100$ system, deformed and spherical states can coexist [12,13].

We propose here the $A = 116$ [$^{116}\text{Cd}(0^+) - ^{116}\text{In}(1^+) - ^{116}\text{Sn}(0^+)$] system, which displays vibrational properties [14,15] more clearly than the $A = 100$ system, as a better system to test QRPA calculations [16,17]. There is another interesting feature about the $A = 116$ system. The recently measured values of the 2ν -decay half-life of ^{116}Cd , $t_{1/2} = (2.2_{-0.4}^{+0.7}) \times 10^{19}$ yr [18] and $t_{1/2} = [3.75 \pm 0.35(\text{stat}) \pm 0.21(\text{syst})] \times 10^{19}$ yr [19], and the experimentally extracted Gamow-Teller strengths [20] can be compared to an estimation of the contribution of the virtual transition via only the ground state (g.s.) of ^{116}In (see Fig. 1). The decay rate is given by

$$[t_{1/2}^{(2\nu)}]^{-1} = G^{2\nu} |M_{\text{GT}}^{(2\nu)}|^2, \quad (1)$$

where $G^{2\nu}$ corresponds to the phase space and we approximate $M_{\text{GT}}^{(2\nu)}$ as

$$M_{\text{GT}}^{(2\nu)} = \frac{\langle ^{116}\text{Sn}(\text{g.s.}) \| \sigma \tau^- \| ^{116}\text{In}(\text{g.s.}) \rangle \langle ^{116}\text{In}(\text{g.s.}) \| \sigma \tau^- \| ^{116}\text{Cd} \rangle}{(Q_{\text{EC}^+} + Q_{\beta^-})/2m_e}. \quad (2)$$

*Present address: MIT-Bates Linear Accelerator Center, Middleton, MA 01949.

The ft value for the β^- transition from the g.s. of ^{116}In to the g.s. of ^{116}Sn is known [21], but the electron-capture- (EC-) decay branch to the g.s. of ^{116}Cd is not known. If we assume it to be similar to the corresponding transition in the neighboring nucleus ^{114}Cd , i.e., $\log ft=4.9$, we obtain $t_{1/2}^{(2\nu)} = 4.81 \times 10^{19}$ yr ($g_A=1$). This shows that the contribution from the ground state of ^{116}In alone could approximately account for the total decay rate. A similar argument was presented by Abad *et al.* [22] who proposed that the situation could be common to all $0^+ \rightarrow 0^+$ double- β -decaying nuclei in which the ground state of the intermediate nucleus has $J^\pi=1^+$. The $A=100$ system was found to be consistent with this hypothesis [23]. The fact that the transition through the ground state of the intermediate nucleus dominates the double- β -decay rate shows that it is important for the calculations to reproduce the single- β -decay matrix elements that connect this state to the double- β -decay initial and final states. In the following section we describe two experiments we performed to measure the EC decay branch of ^{116}In .

II. EXPERIMENT

We produced ^{116}In by means of the $^{115}\text{In}(d,p)$ reaction using a 7.6-MeV deuteron beam from the Notre Dame FN Tandem accelerator. The beam impinged on a stack of four $\approx 100 \mu\text{g}/\text{cm}^2$ In targets evaporated on $5 \mu\text{g}/\text{cm}^2$ carbon foils. In order to reduce the background from the $\text{In}(K\alpha)$ x rays which are profusely produced by particle or photon excitation of the In targets, a He-jet system was used to transport the radioactivity to a remote shielded counting station. The radioactivity from the He jet was deposited onto a paper tape which was moved after a length of time (which we shall refer to as the cycle length) by a tape drive unit and was positioned at our counting station (see Fig. 2). Our detection system consisted of a planar Ge detector (x-ray detector) to detect Cd x rays ($E_x \approx 23$ keV), which constitute the signature of the EC decays of ^{116}In , and an annular high-purity Ge detector (γ -ray detector) to detect ^{116}In γ rays following the β^- decay of ^{116}In in which we used to determine the number of ^{116}In atoms transported to our counting station. In addition we recorded for every event the time interval between the

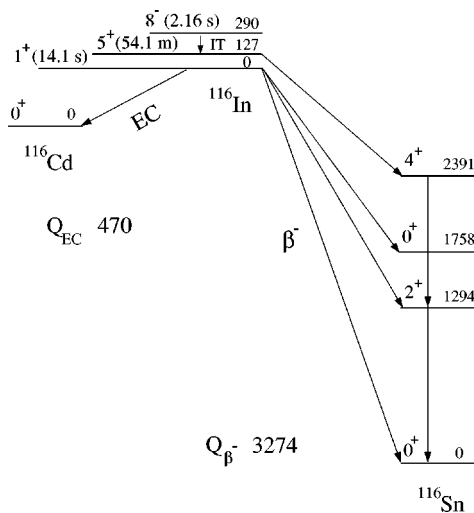


FIG. 1. Decay scheme of the $A=116$ system relevant to the present work. All energies are in keV.

start of the counting cycle, i.e., positioning of the fresh radioactivity in place, and the detection of a signal in the x-ray or the γ -ray detector. This was done by recording for every event the readout of a scaler which was zeroed every time fresh radioactivity was positioned at the counting station and was incremented by a clock.

We performed a first experiment using natural In (95.7% ^{115}In +4.3% ^{113}In) targets, and later a second experiment with ^{115}In targets of 99.99% isotopic purity. In the following sections we present the results of the two experiments separately.

A. Experiment with ^{nat}In targets

We collected our data in four sets with four different cycle lengths for the following reasons. A 4-s cycle was used to obtain data from the decay of the isomer $^{116}\text{In}^{m2}$ ($t_{1/2}=2.18$ s) to obtain the x-ray line-shape parameters. A 30-s cycle was used to optimize the Cd x rays from the EC decay of ^{116}In ($t_{1/2}=14.1$ s). A 100-s cycle was used, in conjunction with the 30-s cycle, to determine the fraction of Cd x rays from the decay of ^{116}In as compared to those from the decay of ^{114}In ($t_{1/2}=71.9$ s). This optimum value of 100 s was obtained from Monte Carlo calculations. Figure 3 shows the simulated error in the ratio of the intensities of the x-rays from ^{114}In and ^{116}In vs the cycle length. Finally we used a 2-h cycle to determine the number of $^{116}\text{In}^{m1}$ transported to our counting station.

1. X-ray spectrum line shape

Figure 4 shows the the x-ray spectrum for the 4-s cycle. The spectrum shows x rays from the internal conversion (i.c.) of the $8^- \rightarrow 5^+$ isomeric transition γ ray. We fitted the spectrum using a line shape characterized by a Gaussian with a low-energy exponential tail plus a flat plateau to take into account incomplete charge collection and Compton scattering, respectively. Figure 4 also shows the best fit to this spectrum obtained by fixing the relative intensities of the $K\alpha_1$, $K\alpha_2$, $K\beta_1$, and $K\beta_2$ In x rays according to the tables of Ref. [21]. We use the parameters obtained from this fit as our line shape parameters.

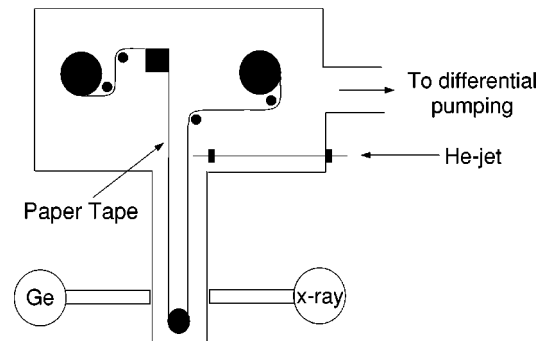


FIG. 2. Schematic diagram of the experimental setup. The radioactivity was transported from the production site via the He-jet system and was deposited onto the paper tape. The paper tape was then moved to position the radioactivity in front of the x-ray detector.

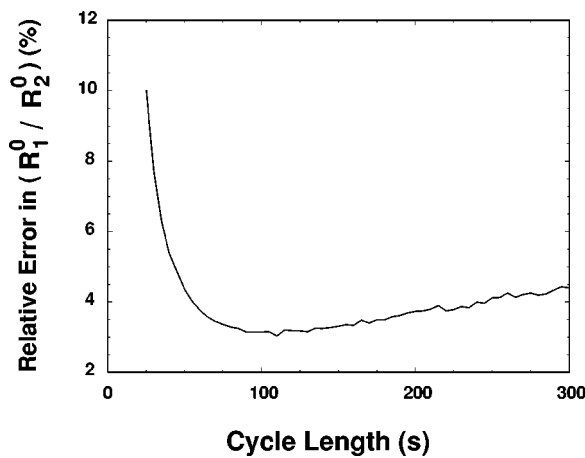


FIG. 3. Monte Carlo simulation of the uncertainty in the ratio of the intensities of Cd x rays from ^{116}In EC decays and ^{114}In EC decays as a function of the cycle length. We chose to run at a cycle length of 100 s to minimize this uncertainty.

2. Efficiency of the x-ray detector

In order to calculate the EC branch, we determined the relevant detector efficiencies in the following way.

(i) We used the 4-s cycle data, dominated by $^{116}\text{In}^{m2}$ decays, to measure the efficiency of the x-ray detector for the $\text{In}(K\alpha)$ x rays relative to the efficiency of the γ -ray detector for the 162-keV γ ray which this source produces with known relative intensities [24].

(ii) We then used a calibrated ^{133}Ba source to measure the absolute efficiency of the γ -ray detector for the 160-keV γ ray and using the previous ratio we obtained the absolute efficiency of the x-ray detector for the $\text{In}(K\alpha)$ x ray. Although we need the efficiency of the x-ray detector for the $\text{Cd}(K\alpha)$ x ray to calculate the EC branch, it is sufficient to use the efficiency for the $\text{In}(K\alpha)$ x ray as the change in efficiency of the x-ray detector for such a change in energy is negligible.

(iii) Finally we used a calibrated ^{60}Co source to interpolate the absolute efficiency of the γ -ray detector for $E_\gamma = 1294$ keV using a $1/E_\gamma$ interpolation between the two ^{60}Co lines.

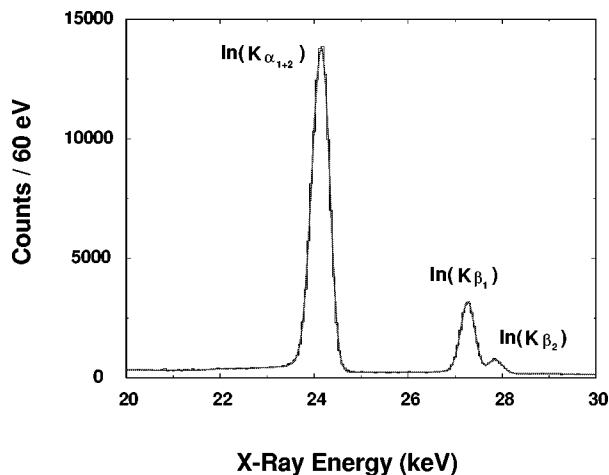


FIG. 4. X-ray spectrum for the 4-s cycle with $^{\text{nat}}\text{In}$ targets. This spectrum was used to determine the line-shape parameters. The fit to the data is shown.

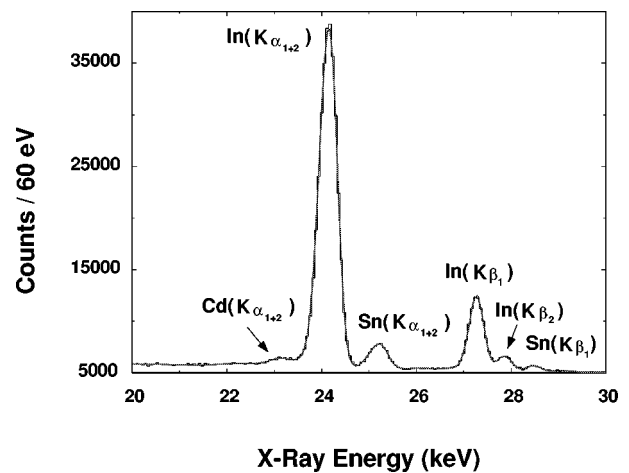


FIG. 5. X-ray spectrum for the 30-s cycle with $^{\text{nat}}\text{In}$ targets. The solid line shows the fit using the parameters obtained from the 4-s cycle data.

In this way we determine the ratio $\eta(\text{In } K\alpha \text{ x ray}) / \eta(1294\text{-keV } \gamma \text{ ray}) = (3.58 \pm 0.34)$ that we use for calculating the EC branch. Here $\eta(E)$ is the photopeak efficiency at energy E .

3. EC decay of ^{116}In

The number of EC decays of ^{116}In can be counted by counting the Cd x rays. Figure 5 shows the x-ray spectrum for the 30-s cycle and Fig. 6 shows that for the 100-s cycle. In order to minimize the signal-to-noise ratio, we incremented the spectrum in Fig. 5 only with events that occurred 2.5 s after positioning the radioactivity. The $\text{Cd}(K\alpha)$ x rays can be clearly seen in both spectra. Also shown in these figures are the fits to the spectra using the line-shape parameters obtained from the 4-s cycle data. In this way we obtained (3259 ± 254) and (3217 ± 259) as the number of $\text{Cd}(K\alpha)$ x rays for the 30-s and 100-s cycles, respectively.

4. Cd x rays from ^{114}In EC decays

Our experiment has a relatively low level of contamination from other products of the $^{115}\text{In} + d$ reaction, because

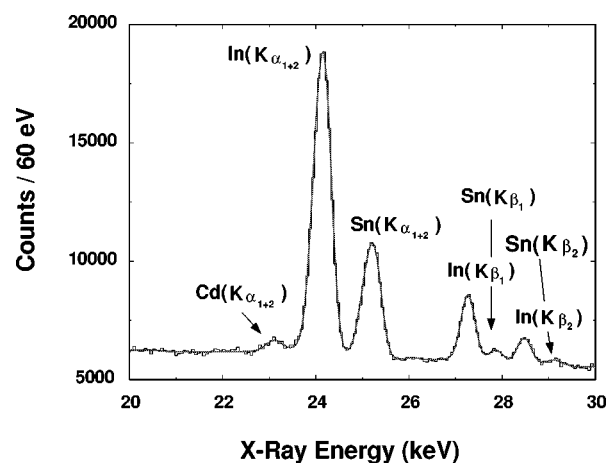


FIG. 6. X-ray spectrum for 100-s cycle with $^{\text{nat}}\text{In}$ targets. The solid line shows the fit using the parameters obtained from the 4-s cycle data.

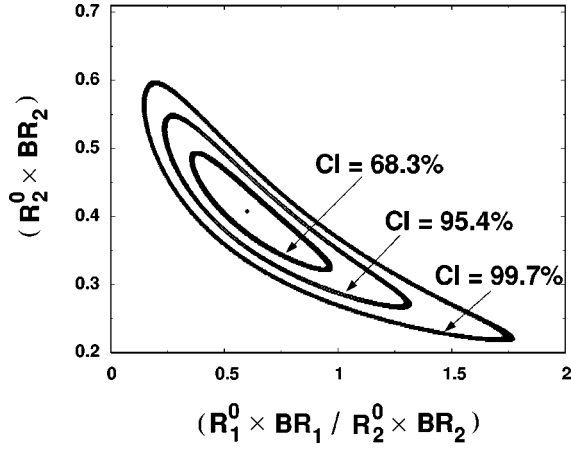


FIG. 7. Iso- χ^2 contour plots for various confidence levels on a $(R_2^0 \times BR_2)$ vs $[(R_1^0 \times BR_1)/(R_2^0 \times BR_2)]$ grid. The result was used to separate the contributions of ^{116}In EC decay from those of ^{114}In EC decay to the Cd x-ray peak.

most of the open channels produce stable isotopes and there are no known, short-lived, low-lying Cd isomers that could produce x rays by internal conversion. Because our targets contained ^{113}In , we produced ^{114}In via $^{113}\text{In}(d,p)$, which has a $\approx 0.46\%$ EC branch. We estimated the ratio of Cd x rays from ^{116}In to ^{114}In by assuming the ratio of the deposition rates for the two isotopes (R_1^0/R_2^0) to be a constant and using the procedure described below.

We divided the total x-ray spectrum for the 30-s cycle into six time bins; i.e., we generated six x-ray spectra for this cycle, the first one corresponding to events occurring within the first 4.64 s after the radioactivity was positioned, the second one corresponding to events occurring between 4.64 and 9.28 s, and so on. Similarly, the total x-ray spectrum for the 100-s cycle was divided into six time bins, each 16.4 s wide. We fitted the time-binned Cd x-ray areas $A^T(t)$ using a fit function of the following form:

$$A^T(t) = \eta \left[(R_1^T \times BR_1) \frac{(1 - e^{-\lambda_1 \Delta T})}{\lambda_1} e^{-\lambda_1 t} + (R_2^T \times BR_2) \frac{(1 - e^{-\lambda_2 \Delta T})}{\lambda_2} e^{-\lambda_2 t} \right], \quad (3)$$

where t stands for the beginning time of a given bin, ΔT is the bin width for a particular cycle, η is the x-ray detector efficiency for Cd x rays, $\lambda_{1,2}$ are the decay constants, and $R_{1,2}^T$ are the rates at the beginning of the counting cycles. The latter are related to $R_{1,2}^0$ in the following way:

$$R_i^T = R_i^0 (1 - e^{-\lambda_i T}) e^{-\lambda_i t_m}, \quad (4)$$

where T is the cycle length and t_m the transport time. We then assumed values of $(R_1^0 \times BR_1)$ and $(R_2^0 \times BR_2)$ on a grid and computed the summed χ^2 for the two cycles. Because we were interested in the ratio $(R_1^0 \times BR_1)/(R_2^0 \times BR_2)$, we plotted contours of equal χ^2 in a $(R_2^0 \times BR_2)$ vs $(R_1^0 \times BR_1)/(R_2^0 \times BR_2)$ grid. The result is shown in Fig. 7. The best value ($\chi^2/\nu = 1.5$) for this ratio obtained in this way was

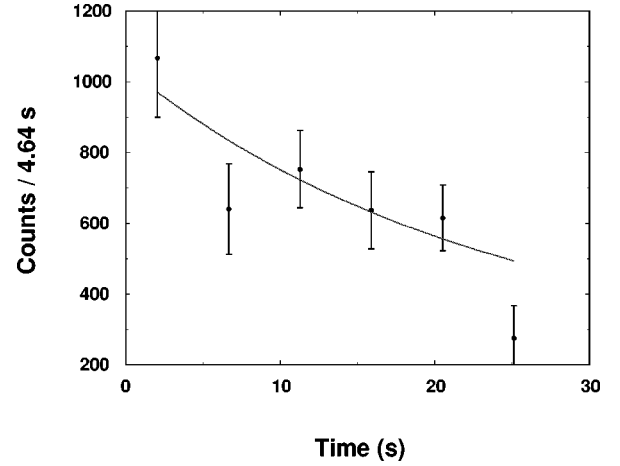


FIG. 8. Time-binned Cd x-ray areas vs time for 30-s cycle with ^{nat}In targets. The solid line shows the fit using the parameters obtained from the grid search.

$$\left(\frac{R_1^0 \times BR_1}{R_2^0 \times BR_2} \right) = 0.60_{-0.25}^{+0.35}. \quad (5)$$

In order to simplify further calculations we use the following number with symmetric error bars which encompass the same region:

$$\left(\frac{R_1^0 \times BR_1}{R_2^0 \times BR_2} \right) = 0.65 \pm 0.30. \quad (6)$$

It can be seen in Fig. 7 that the error in this ratio is asymmetric and that this ratio is not consistent with zero even at the 99.7% confidence level. Figures 8 and 9 show the time-binned Cd x-ray areas for 30-s and 100-s cycles, fitted with exponentials using the parameters obtained with the above procedure.

We now express the total number of Cd x rays observed during each cycle as a function of the deposition rates of the two isotopes, which we will eventually use in conjunction with Eq. (6) to obtain the number of Cd x rays from the

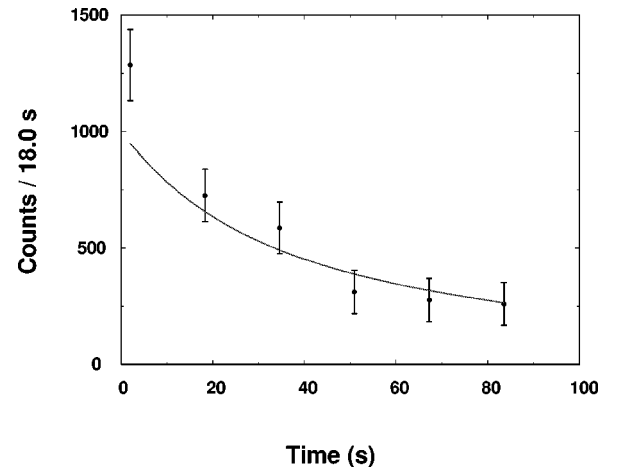


FIG. 9. Time-binned Cd x-ray areas vs time for 100-s cycle with ^{nat}In targets. The solid line shows the fit using the parameters obtained from the grid search.

decay of ^{116}In , as follows. The number of Cd x rays, N^T , produced in front of the x-ray detector during N_C^T cycles of length T is given by

$$N^T = N_C^T \times a^T \times (R_1^0 \times \text{BR}_1 \times C_1^T + R_2^0 \times \text{BR}_2 \times C_2^T), \quad (7)$$

with

$$C_i^T = \frac{1}{\lambda_i} (1 - e^{-\lambda_i T}) e^{-\lambda_i t_m} (1 - e^{-\lambda_i (T - t_m)}), \quad (8)$$

where a^T are constants which take into account the difference in the absolute deposition rates (which depend, among other things, on the beam intensity and the transport efficiency of the He-jet system) for the 30-s and 100-s cycles. The first factor in the above expression corresponds to the number of atoms deposited, the second factor takes into account the number that decays while the tape is moving, and the third factor yields the fraction that decays in front of the detector. From the total number of 160-keV isomeric transition (IT) γ rays and the total number of (fixed frequency) pulser counts observed in the 30-s and 100-s cycles we determined

$$\left(\frac{a^{30} \times N_C^{30}}{a^{100} \times N_C^{100}} \right) = 5.48 \pm 0.16. \quad (9)$$

Finally we calculated the ratio of the number of Cd($K\alpha$) x rays from the decay of ^{116}In to the total number of Cd($K\alpha$) x rays, using Eqs. (7) and (6), to be

$$\left(\frac{N^{30}({}^{116}\text{Cd})}{N^{30}} \right) = 0.52 \pm 0.27 \quad (10)$$

and

$$\left(\frac{N^{100}({}^{116}\text{Cd})}{N^{100}} \right) = 0.24 \pm 0.11, \quad (11)$$

in the 30-s and 100-s cycles, respectively. This implies that for the 30-s cycle (excluding the first 2.5 s after the radioactivity was positioned, as explained in the previous subsection) we have (1695 ± 890) Cd($K\alpha$) x rays and for the 100-s cycle (772 ± 359) Cd($K\alpha$) x rays from ^{116}In EC decays.

5. Test of our half-life measurement procedure

To check our half-life measurement procedure we measured the half-life of $^{116}\text{In}^{m2}$ using the 30-s cycle data. We binned the area for the In x ray in six time bins and fit it with two exponentials as shown in Fig. 10. A second exponential with a long half-life (but small amplitude) is required for a good fit to the data. We assume the origin for these long-lived In x rays to be internal conversion of γ -ray transitions from the higher-excitation-energy isomers of ^{116}In as well as those from $^{114}\text{In}^m$. In this way we obtain

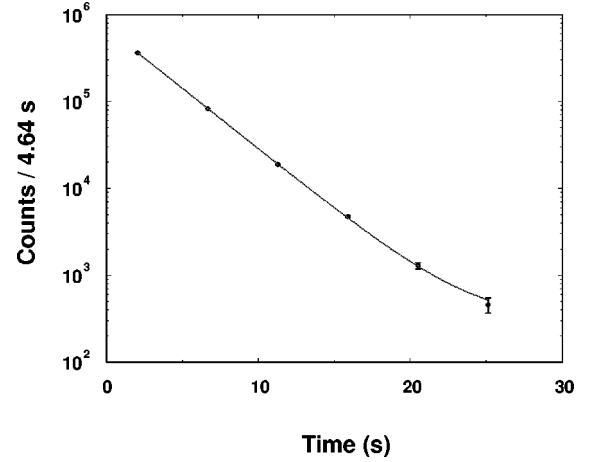


FIG. 10. Fit to the time-binned In x-ray areas for the 30-s cycle.

$$t_{1/2}({}^{116}\text{In}^{m2}) = (2.16 \pm 0.01) \text{ s}, \quad (12)$$

which agrees well with the accepted value of (2.18 ± 0.04) s from Ref [25].

6. Determination of the EC decay branch

The total number of ^{116}In atoms transported to our counting station can be deduced from the total number of 1097-keV γ rays (due only to β^- decays of $^{116}\text{In}^{m1}$) and 1294-keV γ rays (due to β^- decays of $^{116}\text{In}^{m1} + {}^{116}\text{In}$) (see Fig. 11). To determine the number of 1294-keV γ rays from ^{116}In decays, we compared the ratio of the number of the two γ rays for the 30-s and 100-s cycle runs to the same ratio measured for the 2-h cycle run (the counting for this run began sufficiently late and hence had a negligible contribution from ^{116}In decay). The ratio of the number of the 1294-keV to the 1097-keV γ rays from this 2-h cycle was 1.264 ± 0.004 . The same ratio for the 30-s and 100-s cycles was (1.654 ± 0.007) and (1.297 ± 0.009) , respectively. These ratios, corrected for small summing effects, allowed us to determine the fraction of 1294-keV γ rays from ^{116}In to be (0.240 ± 0.004) and (0.026 ± 0.001) for the 30-s and 100-s cycles, respectively.

Finally we calculate the EC decay branch using

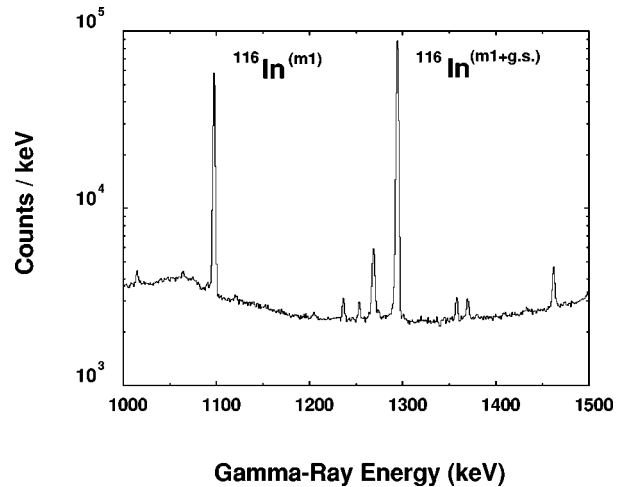


FIG. 11. γ -ray spectrum for the 30-s cycle with ^{nat}In targets.

$$\text{BR(EC)} = \frac{A(\text{Cd } K\alpha \text{ x ray}) \eta(1294 \text{ keV } \gamma) \text{BR}(1294 \text{ keV})}{A(1294 \text{ keV from } ^{116}\text{In}) \eta(\text{Cd } K\alpha \text{ x ray}) P_K \omega_{K\alpha}}, \quad (13)$$

where $\eta(\text{In } K\alpha \text{ x ray})/\eta(1294\text{-keV } \gamma \text{ ray}) = (3.58 \pm 0.34)$ is the ratio of the detector efficiencies, $\text{BR}(1294 \text{ keV}) = 1.3\%$ is the probability of the emission of a 1294-keV γ ray in a β^- decay of ^{116}In , $P_k = 0.85$ is the fraction of EC decays that produce a vacancy in the K shell, and $\omega_{K\alpha} = 0.70$ is the $K\alpha$ fluorescence yield, i.e., the probability of the emission of a $\text{Cd}(K\alpha)$ x-ray per K vacancy [25]. We thus obtain

$$\text{BR(EC)} = (1.94 \pm 1.04) \times 10^{-2}\%. \quad (14)$$

B. Experiment with isotopically enriched ^{115}In targets

In this run we used the same experimental setup as in the first experiment except for the fact that the γ -ray detector was moved closer to and the x-ray detector was accidentally moved farther from the source spot. However, because in this case we were not concerned with ^{114}In contamination, which would give rise to a long-lived component to the Cd x rays, we used only three cycle lengths, viz., 4-s, 30-s, and 2-h cycles to collect our data.

1. Efficiencies

Like in the previous experiment, in order to calculate the EC branch, we used the ratio of the efficiency of the x-ray detector for the $\text{In}(K\alpha)$ x ray to the efficiency of the γ -ray detector for the 1294-keV γ ray. Using the same procedure as before we obtained the relative efficiency to be $\eta(\text{In } K\alpha \text{ x ray})/\eta(1294\text{-keV } \gamma \text{ ray}) = (0.91 \pm 0.09)$. The significant decrease in this ratio compared to the first experiment was due to higher efficiency for the γ -ray detector and lower efficiency for the x-ray detector.

2. Determination of the EC decay branch

Figure 12 shows the x-ray spectrum for the 4-s cycle,

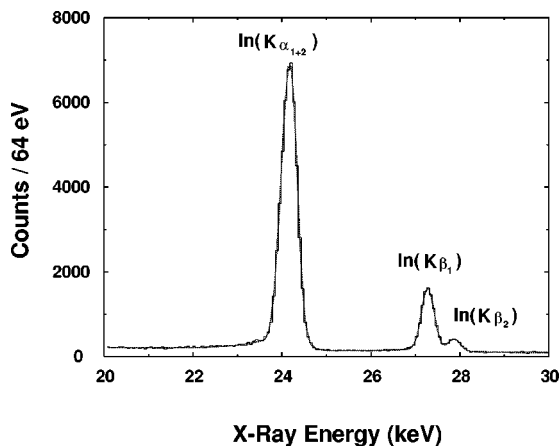


FIG. 12. X-ray spectrum for the 4-s cycle with isotopically enriched ^{115}In targets. This spectrum was used to determine the line-shape parameters. The fit to the data is shown.

which was used to obtain line-shape parameters, and Fig. 13 shows the x-ray spectrum for the 30-s cycle. From this spectrum we obtained (1541 ± 385) as the number of $\text{Cd}(K\alpha)$ x rays. We then used the same procedure as for the first experiment to obtain the number of ^{116}In atoms transported to the counting station using the γ -ray spectra. Finally using the number of $\text{Cd}(K\alpha)$ x rays and the number of ^{116}In atoms transported to the counting station we obtained the EC decay branch of ^{116}In to be $(2.46 \pm 0.80) \times 10^{-2}\%$. This value for the EC branch is in good agreement with the value from the previous experiment.

In order to estimate the half-life corresponding to the Cd x rays, we divided the total x-ray spectrum into three time bins, each 9.4 s wide, and fitted them with one exponential. We obtained $t_{1/2} = 27.4 \pm 49.8$ s. Figure 14 shows the time-binned areas along with the best fit (solid line) and the fit assuming the half-life to be 14.1 s (dashed line). It is clear from the figure that due to large uncertainties in the areas it is not possible to clearly establish the half-life of these x rays.

C. Average and adopted value for the ^{116}In EC branch

The average (weighted by the errors) of the EC branch obtained from the two experiments is $(2.27 \pm 0.63) \times 10^{-2}\%$. We adopt this value as the EC branch of ^{116}In . Using this branch and the well-known half-life of ^{116}In we obtain, $\log ft = 4.39^{+0.10}_{-0.15}$, where the phase space factor f was obtained according to the tables of Ref. [26].

III. QRPA CALCULATIONS

We performed calculations in a basis consisting of two complete oscillator shells around the double-shell closure $N = Z = 50$, assuming ^{40}Ca as the inert core. The energy levels were taken as those of an effective Woods-Saxon potential including Coulomb effects. We used the effective two-body interaction from Ref. [27] with proton and neutron pairing

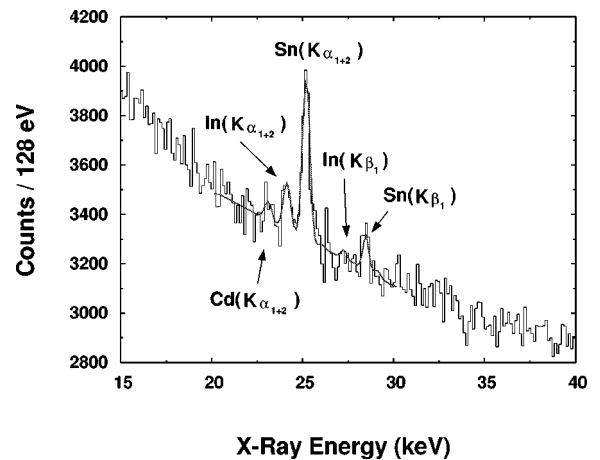


FIG. 13. Last 9.4 s of the x-ray spectrum for the 30-s cycle with isotopically enriched ^{115}In targets. The fit to the data is shown.

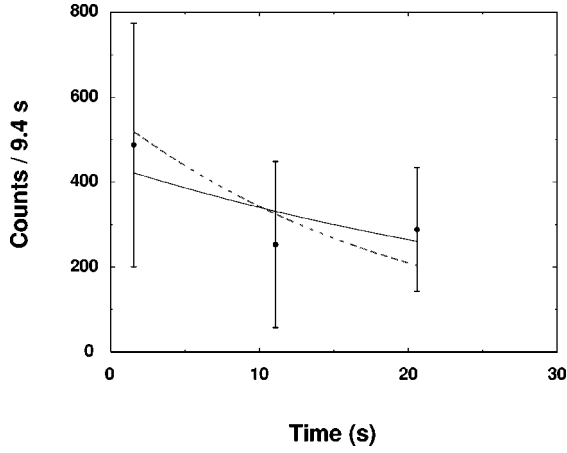


FIG. 14. Time-binned Cd x-ray areas for the 30-s cycle with isotopically enriched ^{115}In targets. The figure shows the best fit ($t_{1/2} = 27.4 \pm 49.8$ s) to the data and the fit with the half-life fixed to that of ^{116}In ($t_{1/2} = 14.1$ s).

terms included. The coupling constants of the pairing channels of the interaction were adjusted to reproduce the observed mass differences, both for proton and neutron states around the initial (^{116}Cd) and final (^{116}Sn) nucleus.

The set of virtual intermediate states needed to calculate the double- β -decay matrix elements are described as the superposition of quasiproton and quasineutron pairs coupled to angular momentum $J^\pi = 1^+$ and with eigenvalues and amplitudes given by the proton-neutron-QRPA (pn -QRPA) model [7,8,28]. The input for the pn -QRPA calculations is quasiparticle energies and occupation numbers as well as the coupling constants governing particle-hole and particle-particle channels of the two-body interaction. The strength of the proton-neutron particle-hole channels was adjusted to reproduce the energy of the giant Gamow-Teller (GT) resonance. Our value for the energy of the GT resonance in ^{116}In is about $E_{\text{GT}} = 15$ MeV, measured from the ground state of In. The strength of proton-neutron particle-particle channels of the interaction, g_{pp} , is determined via the known single- β -decay transitions in ^{116}In . As usual in these kinds of calculations two sets of pn -QRPA states have to be built, one describing the excitations starting from the initial nucleus and the other corresponding to excitations starting from the final nucleus, both interpreted as states of the intermediate nucleus. Wave functions and overlaps between both sets of states are treated as in [7]. The excited states of ^{116}Sn are described as the superposition of two quasiprotons and two quasineutrons. The QRPA matrix equations are diagonalized to determine amplitudes and eigenvalues for monopole and quadrupole excitations. The energy of the first excited quadrupole state and the value of the measured $B(E2)$ transition from this state to the ground state are reproduced in the calculations by adjusting the coupling constant of the quadrupole channels of the two-body interaction and by introducing effective charges [29]. The results of the present calculation are $B(E2, 2_1^+ \rightarrow 0_{\text{g.s.}}^+) = 10.6$ Weisskopf units (W.u.), for $e_{\text{eff}}^{(\text{p})} = 1.39e$ and $e_{\text{eff}}^{(\text{n})} = 0.39e$. For the monopole excitations it has been verified that the first QRPA eigenvalue, at zero energy, is just the solution of the pairing-gap equation corresponding to the same interaction.

TABLE I. Experimental and theoretical excitation energies and $\log ft$ values corresponding to low-lying states of ^{116}Sn . The states at 2.58 MeV are the members of the two-quadrupole-phonon triplet.

J^π	Experimental values [36]		Theory		
	Energy [MeV]	$\log ft$	Energy [MeV]	$\log ft$	
				$g_{\text{pp}} = 1.00$	$g_{\text{pp}} = 0.75$
$0_{\text{g.s.}}^+$	0.0	4.66	0.0	5.32	4.66
2_1^+	1.29	5.85	1.29	5.18	5.20
0_1^+	1.76	5.88	1.71	5.23	5.21
0_2^+	2.03	—	2.58	6.25	6.24
2_2^+	2.11	6.31	2.58	6.84	6.81
2_3^+	2.23	6.40	2.35	6.94	6.91
4_1^+	2.39	—	2.58		
0_3^+	2.55	5.99	2.57	4.14	4.15
2_4^+	2.65	5.79	2.49	5.84	5.92

The $\log ft$ values of both the β^- and β^+/EC allowed transitions are defined by

$$\log ft = \ln \left(\frac{6147}{B(\text{GT})} \right), \quad (15)$$

where

$$B(\text{GT}) = g_A^2 \frac{|\langle J_f || \sigma \tau^- || J_i \rangle|^2}{(2J_i + 1)}. \quad (16)$$

The results of the QRPA calculations, for the excitation energies of and β^- $\log ft$ values to, states in ^{116}Sn are shown in Table I. In the calculations we have used the value of $g_A = 1.0$, for the axial-vector coupling constant [17]. The two sets of calculated values correspond to $g_{\text{pp}} = 0.75$ and $g_{\text{pp}} = 1.0$, respectively. The first value ($g_{\text{pp}} = 0.75$) reproduces the data on the β^- branch of the decay of the ground state of ^{116}In whereas the other value ($g_{\text{pp}} = 1.0$), corresponding to the unrenormalized two-body interaction, yields a better agreement with data for the double- β -decay transition to the ground state of ^{116}Sn . As seen from the results shown in this table, the change in the value of g_{pp} does not affect much the values of the matrix elements for single- β -decay transitions, except for the value corresponding to the feeding of the ground state of ^{116}Sn . This is a manifestation of the effects on the wave functions of virtual intermediate one-phonon states due to proton-neutron two-particle correlations. Concerning the EC feeding of the ground state of ^{116}Cd from the ground state ($J^\pi = 1^+$) of ^{116}In the theoretical values are $\log ft = 4.19$ ($g_{\text{pp}} = 0.75$) and $\log ft = 4.0$ ($g_{\text{pp}} = 1.0$), which can be compared with the presently measured value $\log ft = 4.39_{-0.15}^{+0.10}$.

The general expression for the matrix element governing the two-neutrino mode of the nuclear double β decay, from an initial 0^+ ground state (A, N, Z) to a final J_f^+ state ($A, N - 2, Z + 2$), is given by

$$M_{\text{GT}}^{(2\nu)}(J_f^+) = \sum_m \frac{\beta_m^{(f)}(J_f^+) \beta_m^{(i)}}{[(\frac{1}{2} Q_{\beta\beta} + E_m - M_i)/m_e + 1]^s}, \quad (17)$$

TABLE II. Theoretical matrix elements $M_{\text{GT}}^{(2\nu)}$ and half-lives $t_{1/2}^{(2\nu)}$ for the $2\nu\beta\beta$ decay of ^{116}Cd to various final states of ^{116}Sn . The matrix elements $M_{\text{GT}}^{(2\nu)}$ are given in units of $(m_e)^{-1}$. The corresponding phase space factors $G_{\text{GT}}^{(2\nu)}$ are given in units of yr^{-1} .

Transition	$G_{\text{GT}}^{(2\nu)}$	$M_{\text{GT}}^{(2\nu)}$		$t_{1/2}^{(2\nu)}$ (yr)	
		$g_{\text{pp}}=1.00$	$g_{\text{pp}}=0.75$	$g_{\text{pp}}=1.00$	$g_{\text{pp}}=0.75$
$0_{\text{g.s.}}^+ \rightarrow 0_{\text{g.s.}}^+$	2.99×10^{-18}	0.12	0.21	2.33×10^{19}	0.76×10^{19}
$0_{\text{g.s.}}^+ \rightarrow 2_1^+$	2.33×10^{-21}	0.021	0.016	1.0×10^{24}	1.7×10^{24}
$0_{\text{g.s.}}^+ \rightarrow 0_1^+$	8.98×10^{-22}	0.31	0.26	1.16×10^{22}	1.6×10^{22}
$0_{\text{g.s.}}^+ \rightarrow 0_{2\otimes 2}^+$	8.90×10^{-23}	0.13	0.11	6.63×10^{23}	1.0×10^{24}

where $s=1$ for $J=0$ and $s=3$ for $J=2$, and the sum extends over all 1^+ states of the intermediate nucleus. The denominator of this equation consists of the energy E_m of the m th intermediate 1^+ state and the mass energy M_i of the parent nucleus, as well as of the double- β -decay Q value, $Q_{\beta\beta}$. The virtual single- β -decay matrix elements of $M_{\text{GT}}^{(2\nu)}(J_f^+)$ are defined in [30,31] and the overlaps between the two sets of pn -QRPA solutions are added to account for the matching of the intermediate 1^+ states [7].

The structure of the matrix elements, for virtual single- β -decay transitions from a pn -phonon state to a $pp+nn$ -phonon state, is given in [28,30–32] and the double- β -decay half-life $t_{1/2}^{(2\nu)}$ can be obtained from the expression

$$[t_{1/2}^{(2\nu)}(0_{\text{g.s.}}^+ \rightarrow J_f^+)]^{-1} = |M_{\text{GT}}^{(2\nu)}(J_f^+)|^2 G_{\text{GT}}^{(2\nu)}(J_f^+), \quad (18)$$

where J_f^+ can either be the ground state or an excited state of the double- β -decay daughter and the integrated kinematical factors $G_{\text{GT}}^{(2\nu)}(J_f^+)$ can be calculated as described in [33]. These factors are given in Table II.

The pn -QRPA calculations, for $g_{\text{pp}}=1.0$, yield a final matrix element $M_{\text{GT}}^{(2\nu)}=0.120$ (in units of inverse electron mass) for the transition to the ground state of ^{116}Sn . This result is practically given by the contribution of a single virtual excitation. Slightly weaker dominance is found in the results corresponding to $g_{\text{pp}}=0.75$. In the framework of the pn -QRPA it corresponds to the contribution of the first excited 1^+ state of ^{116}In , relative to the ground state of both the initial and final nuclei. Because the ground state of ^{116}In is a 1^+ state, this result supports the so-called single-state dominance, which postulates that when the ground state of the intermediate nucleus in a double- β -decay chain is a 1^+ state, then the value of the matrix element $M_{\text{GT}}^{(2\nu)}$ would be given by the contribution of this single state. In practice two effects are contributing to this dominance, namely, (a) that the contribution of the virtual 1^+ excitation has a small energy denominator when this state is also the ground state, and (b) that the product of single- β -decay matrix elements entering in the definition of $M_{\text{GT}}^{(2\nu)}$ is mostly governed by the virtual β^+ transition. As explained in [34] and in [35] proton-neutron two-particle correlations produce a destructive interference between the β^- and β^+ branches of the virtual decay path.

When the matrix element $M_{\text{GT}}^{(2\nu)}$ is approximated by the product of the matrix elements extracted from the measured β^- [36] and the presently measured EC transition one gets

the value $(M_{\text{GT}}^{(2\nu)})_{\text{approx}}=0.15 \pm 0.04$, in agreement with the above-reported theoretical value. With this result and using Eq. (1) one gets

$$t_{1/2}^{2\nu}(0_{\text{g.s.}}^+ \rightarrow 0_{\text{g.s.}}^+) = (1.49 \pm 0.41) \times 10^{19} \text{ yr}. \quad (19)$$

As shown in Table II, the matrix elements for transitions to the ground state and to the first excited 0^+ state, described as a one-phonon monopole excitation, are of the same order of magnitude. However, because of phase space limitations, the corresponding half-life is longer than the half-life for the ground-state transition but still not so long as the ones for the quadrupole one- and two-phonon states (denoted as $0_{2\otimes 2}^+$ in Table II). In the context of the present discussion we shall interpret this result as a firm indication of the structure of the first excited 0^+ state as a monopole vibration. The QRPA wave function, for this state, is mainly given by the $(s_{1/2})^2$ and $(d_{3/2})^2$ two-quasineutron configurations.

To conclude with the analysis of the QRPA results it can be said that the overall agreement between data and the calculations, both for the single- and double- β -decay transitions, supports the notion that the theoretical approximations work better in the $A=116$ system than in the $A=100$ system [10,11] where the QRPA was seen to fail in predicting data. This may be due to the fact that both ^{116}Cd and ^{116}Sn are spherical nuclei, a condition which may not be met in the $A=100$ system. In spite of the fact that the theoretical result for the single- β^- -decay rate to the g.s. of ^{116}Sn for $g_{\text{pp}}=1.0$ shows a larger discrepancy with the data than the result obtained for $g_{\text{pp}}=0.75$, both sets of results seem to confirm the single-state dominance on the matrix element $M_{\text{GT}}^{(2\nu)}$.

IV. CONCLUSIONS

We have measured the EC decay branch of ^{116}In to be $(2.27 \pm 0.63) \times 10^{-2}\%$, which implies $\log ft = 4.39_{-0.10}^{+0.10}$. Using our measured $\log ft$ value we obtained $g_A^2 \langle \langle ^{116}\text{In} | \sigma \tau^- | ^{116}\text{Cd} \rangle \rangle^2 = (0.75 \pm 0.21)$, in strong disagreement with the value extracted from $(^3\text{He}, t)$ measurements [20]: (0.032 ± 0.005) . It is not clear what definition of $B(\text{GT})$ the authors of Ref. [20] used, but the disagreement is large in any case. While our experiment is a direct measurement, the charge-exchange measurement is based on assumptions that have been shown to break [37] for weak transitions, like the transition in question. Using this measured value for the matrix element in Eq. (2) and using Eq. (1) we calculate the contribution of the ground state of ^{116}In to the 2ν double- β -decay rate to be

$$t_{1/2}^{(2\nu)}(0_{\text{g.s.}}^+ \rightarrow 0_{\text{g.s.}}^+) = (1.49 \pm 0.41) \times 10^{19} \text{ yr}, \quad (20)$$

which is in reasonable agreement with the measured half-lives [18,19].

This confirms the guess, presented in Sec. I, that the contribution of the ground state of ^{116}In accounts for an important fraction of the 2ν double- β -decay rate of ^{116}Cd . Thus we observe for ^{116}Cd a confirmation of the *low-lying-state dominance hypothesis* suggested by Abad *et al.* [22]. We have also shown that QRPA calculations in this case show a relatively better agreement with measurements as compared to the $A=100$ system. We find agreement with the single- β -decay rates using $g_{\text{pp}}=0.75$, but this value of g_{pp} yields a 2ν -decay rate about 3 times faster than measurement. On the other hand $g_{\text{pp}}=1.0$ gives good agreement with the measured 2ν -decay rate but predicts a β^- -decay rate to ground state of ^{116}Sn about 4 times smaller than its measured value. Nevertheless, both sets of results support the low-lying-state dominance hypothesis concerning the value of the matrix element for the two-neutrino double- β -decay mode.

The 2ν -decay rate of ^{116}Cd to the excited state of ^{116}Sn has not been measured yet. We can make a trivial prediction based on the *low-lying-state dominance hypothesis*, which implies that the 2ν matrix element should be proportional to

$$\frac{M^{(2\nu)}(\text{Sn}^*)}{M^{(2\nu)}(\text{Sn}^{\text{g.s.}})} = \left[\frac{ft(\text{Sn}^{\text{g.s.}})}{ft(\text{Sn}^*)} \right]^{1/2} \left(\frac{Q_{\text{EC}} + Q_{\beta^-}^{\text{g.s.}}}{Q_{\text{EC}} + Q_{\beta^-}^*} \right), \quad (21)$$

which yields

$$t_{1/2}^{(2\nu)}(0_{\text{g.s.}}^+ \rightarrow 0_1^+) = (2.31 \pm 0.64) \times 10^{23} \text{ yr}. \quad (22)$$

On the other hand, the more sophisticated prediction based on QRPA calculations yields (see Table II)

$$t_{1/2}^{(2\nu)}(0_{\text{g.s.}}^+ \rightarrow 0_1^+) = (1.16 \times 10^{22}) \text{ yr} \quad (23)$$

and

$$t_{1/2}^{(2\nu)}(0_{\text{g.s.}}^+ \rightarrow 0_1^+) = (1.6 \times 10^{22}) \text{ yr} \quad (24)$$

for the different values of the particle-particle strength, $g_{\text{pp}}=1.0$ and $g_{\text{pp}}=0.75$, respectively. These predictions can be compared to the experimental limits of Piepke *et al.* [38]:

$$t_{1/2}^{(2\nu)+0\nu}(0_{\text{g.s.}}^+ \rightarrow 0_1^+) > (2.0 \times 10^{21}) \text{ yr}. \quad (25)$$

As seen from the above results the estimation of the half-life for two-neutrino double- β -decay transition to the first excited 0^+ state of ^{116}Sn based on the single-state dominance, Eq. (19), differs from the QRPA results of Eqs. (20) and (21). This is partly due to the fact that the QRPA prediction for the $\log ft$ value of the single- β -decay transition feeding the same state differs from the experimental value, as seen from the results shown in Table I. Inspection of the contributions to the theoretical matrix element $M_{\text{GT}}^{(2\nu)}$ for the transition to the first excited 0^+ , given in Table II, indicates that most of it is due to the contribution of the first $J^\pi=1^+$ state of ^{116}In . A measurement of the 2ν double- β decay to the first excited 0^+ state of ^{116}Sn would help clarify the nuclear structure mechanism which dominates the decay.

ACKNOWLEDGMENTS

We are grateful to I. Ahmad from ANL for lending us the Ge x-ray detector, to J. P. Greene from ANL for making some of the ^{116}In targets for us, and to Rich Waltz for help in the initial setup of the experiment. A.G. thanks A. Aprahamian, W. Haxton, and P. Vogel for fruitful comments. The University of Notre Dame researchers acknowledge support by the NSF and Warren Foundation. O.C. is supported by the CONICET, Argentina, and by Grant No. PICT0079, and J.S. is supported by the Finnish Academy of Science. M.M.H. acknowledges financial support from DOE Nuclear Physics Division Grant No. DE-FG02-96ER 40995. E.B.N. acknowledges financial support from DOE Nuclear Physics Division Grant No. DE-AC03-76SF 00098.

-
- [1] W.C. Haxton and G.J. Stephenson, Jr., *Prog. Part. Nucl. Phys.* **12**, 409 (1984).
 - [2] E. Caurier, F. Nowacki, A. Poves, and J. Retamosa, *Phys. Rev. Lett.* **77**, 1954 (1996).
 - [3] J.A. Halbleib and R.A. Sorensen, *Nucl. Phys.* **A98**, 542 (1967).
 - [4] D. Cha, *Phys. Rev. C* **27**, 2269 (1983).
 - [5] P. Vogel and P. Fisher, *Phys. Rev. C* **32**, 1362 (1985).
 - [6] P. Vogel and M.R. Zirnbauer, *Phys. Rev. Lett.* **57**, 3143 (1986).
 - [7] O. Civitarese, A. Faessler, and T. Tomoda, *Phys. Lett. B* **194**, 11 (1987).
 - [8] J. Suhonen, T. Taigel, and A. Faessler, *Nucl. Phys.* **A486** 91 (1988).
 - [9] K. Muto, E. Bender, and H.V. Klapdor, *Z. Phys. A* **334**, 177 (1989).
 - [10] A. Griffiths and P. Vogel, *Phys. Rev. C* **46**, 181 (1992).
 - [11] J. Suhonen and O. Civitarese, *Phys. Rev. C* **49**, 3055 (1994).
 - [12] D. Troltenier *et al.*, *Z. Phys. A* **338**, 261 (1991).
 - [13] E. Kirchuk, P. Federman, and S. Pittel, *Phys. Rev. C* **47**, 567 (1993).
 - [14] J. Kumpulainen *et al.*, *Phys. Rev. C* **45**, 640 (1992).
 - [15] S. Raman *et al.*, *Phys. Rev. C* **43**, 521 (1991).
 - [16] M. Moe and P. Vogel, *Annu. Rev. Nucl. Part. Sci.* **44**, 247 (1994).
 - [17] J. Suhonen and O. Civitarese, *Phys. Rep.* (to be published).
 - [18] H. Ejiri, K. Fushimi, R. Hazama, K. Nagata, H. Oshumi, K. Okada, and J. Tanaka, *Nucl. Phys. B (Proc. Suppl.)* **35**, 372 (1994).
 - [19] R. Arnold *et al.*, *Z. Phys. C* **72**, 239 (1996).
 - [20] H. Akimune *et al.*, *Phys. Lett. B* **394**, 23 (1997).
 - [21] *Table of Isotopes*, 8th ed., edited by C.M. Lederer and V.S. Shirley (Wiley, New York, 1996).
 - [22] J. Abad, A. Morales, R. Nunez-Lagos, and A.F. Pacheco, *An. Fis., Ser. A* **80**, 9 (1984).
 - [23] A. García *et al.*, *Phys. Rev. C* **47**, 2910 (1993).
 - [24] We found the value for BR[In($K\alpha$)] from Ref. [25], (10.44

- $\pm 0.33\%$, to be in error. Using the value for e_K/γ from Ref. [21] we calculate $\text{BR}[\text{In}(K\alpha)] = (27.1 \pm 3.2)\%$, which we used for our calibration.
- [25] E. Browne and R.B. Firestone, *Table of Radioactive Isotopes* (Wiley, New York, 1986).
- [26] H. Behrens and J. Janecke, *Numerical Tables for Beta Decay and Electron-Capture*, Landolt-Börnstein, New Series, Vol. I/4 (Springer, Berlin, 1969).
- [27] K. Holinde, Phys. Rep. **68**, 121 (1981).
- [28] J. Suhonen, Nucl. Phys. **A563**, 205 (1993).
- [29] A. Bohr and B.R. Mottelson, *Nuclear Structure* (Benjamin, Reading, MA, 1975), Vol. II.
- [30] J. Suhonen and O. Civitarese, Phys. Lett. B **308**, 212 (1993).
- [31] O. Civitarese and J. Suhonen, Nucl. Phys. **A575**, 251 (1994).
- [32] M. Aunola and J. Suhonen, Nucl. Phys. **A602**, 133 (1996).
- [33] M. Doi, T. Kotani, and E. Takasugi, Prog. Theor. Phys. Suppl. **83**, 1 (1985).
- [34] J. Engel, P. Vogel, O. Civitarese, and M.R. Zirnbauer, Phys. Lett. B **208**, 187 (1988).
- [35] M. Ericson, T. Ericson, and P. Vogel, Phys. Lett. B **328**, 259 (1994).
- [36] J. Blachot and G. Marguier, Nucl. Data Sheets **73**, 81 (1994).
- [37] S.M. Austin, N. Anantaraman, and W.G. Love, Phys. Rev. Lett. **73**, 30 (1994).
- [38] A. Piepke *et al.*, Nucl. Phys. **A577**, 493 (1994).